3D-RadVis: Visualization of Pareto Front in Many-Objective Optimization

Amin Ibrahim, IEEE Member
Faculty of Electrical, Computer, and Software Engineering
University of Ontario Institute of Technology
Oshawa, Canada
amin.ibrahim@uoit.ca

Shahryar Rahnamayan, SMIEEE
Faculty of Electrical, Computer, and Software Engineering
University of Ontario Institute of Technology
Oshawa, Canada
shahryar.rahnamayan@uoit.ca

Miguel Vargas Martin, IEEE Member
Faculty of Business and Information Technology
University of Ontario Institute of Technology
Oshawa, Canada
miguel.vargasmartin@uoit.ca

Kalyanmoy Deb, Fellow, IEEE
Faculty of Electrical, Computer, and Computer Engineering
Michigan State University
East Lansing, Michigan, USA
kdeb@egr.msu.edu

Abstract— In many-objective optimization, visualization of true Pareto front or obtained non-dominated solutions is difficult. A proper visualization tool must be able to show the location, range, shape, and distribution of obtained non-dominated solutions. However, existing commonly used visualization tools in many-objective optimization (e.g., parallel coordinates) fail to show the shape of the Pareto front. In this paper, we propose a simple yet powerful visualization method, called 3-dimensional radial coordinate visualization (3D-RadVis). This method is capable of mapping M-dimensional objective space to a 3-dimensional radial coordinate plot while preserving the relative location of solutions, shape of the Pareto front, distribution of solutions, and convergence trend of an optimization process. Furthermore, 3D-RadVis can be used by decision-makers to visually navigate large many-objective solution sets, observe the evolution process, visualize the relative location of a solution, evaluate trade-off among objectives, and select preferred solutions. The visual effectiveness of the proposed method is demonstrated on widely used many-objective benchmark problems containing variety of Pareto fronts (linear, concave, convex, mixed, and disconnected). In addition, we demonstrated the capability of 3D-RadVis for visual progress tracking of the NSGA-III algorithm through generations. It is worthwhile to mention that a suitable visualization is a crucial prerequisite for an effective interactive optimization.

Keywords— Visualization, evolutionary computation; large-scale; many-objective optimization, radial coordinate mapping; RadVis; 3D-RadVis.

I. INTRODUCTION

Nowadays real-world applications are increasingly complex and more encompassing, in the sense that more decision variables are used to model complex situations and more input data and parameters are available to capture the complexity of the problems. Moreover, many of these problems involve optimizing a high number of objectives.

There are many real-world problems with high number of objectives (usually more than 3 objectives). Many of the state-of-the-art many-objective evolutionary optimization algorithms fail to scale with the number of objectives [1, 2] and find well-converged and well-diversified non-dominated solutions. It happens due to the loss of selection pressure in fitness evaluation [3]. In high-dimensional objective space, the proportion of non-dominated individuals in a randomly generated initial population is often higher than 90% [4-6] and this will considerably diminish the selection pressure during the evolutionary process. Moreover, when the distance of nearly converged parent solutions is high, they will likely produce offspring solutions that are far from the true Pareto front [7, 8].

The other main issue in solving many-objective problems is the difficulty of visualization of solutions as it plays a key role for a proper decision making process and also well-understanding of the algorithms. When the number of objectives is four or greater, the visualization of approximation sets is more challenging [9]. There are many two- or three-dimensional data visualization methods used for many-objective optimization. For example, parallel coordinate [10] and Heatmap plots [11] can be used to visualize the distribution, range, and trade-off among solutions of multi-dimensional objectives, but they are often difficult to interpret because solutions are superimposed or arbitrarily ordered [12]. Other methods, such as self-organizing maps [13] and radial coordinate visualization [14], show the distribution and inter-relationship among objectives, however they fail to show the shape and convergence trend of the solution sets.

This paper proposes a novel 3-dimensional radial coordinate visualization method, called 3D-RadVis, which is capable of mapping an M-dimensional Pareto front to a 3-dimensional view while preserving the shape, accuracy, distribution, and convergence trend of the solution sets. The main goal of this paper is to introduce a powerful visualization method that permits many-objective optimization researchers and decision makers to explore and understand the optimization process and results of an algorithm. The 3D-RadVis allows a decision maker to visually navigate large many-objective solution sets and identify one or more preferred optimal solutions. Since 3D-RadVis maps M-dimensional objective to a 3-dimensional

space, decision makers can take advantage of immersive virtual technologies [15-18], such as the CAVE [19] to easily visualize the entire Pareto front from the 3D-RadVis plot and interactively select the ideal solution according to their requirement and budget. Similarly, researchers can use 3D-RadVis to investigate many-objective optimization algorithm's search behavior, parameter specifications, performance comparison, and hopefully develop new algorithms to tackle many-objective optimization problems. Furthermore, a proper visualization tool can open the door for an effective interactive optimization.

The rest of the paper is organized as follows. Section II provides the description of visualization methods used in many-objective optimization. Section III provides the technical description of the proposed visualization scheme, 3D-RadVis. Section IV presents how 3D-RadVis maps the Pareto fronts of well-known many-objective test problems. Conclusion remarks are provided in Section V.

(a) Parallel coordinates plot

(b) Scatter plot matrix

(c) Heatmap

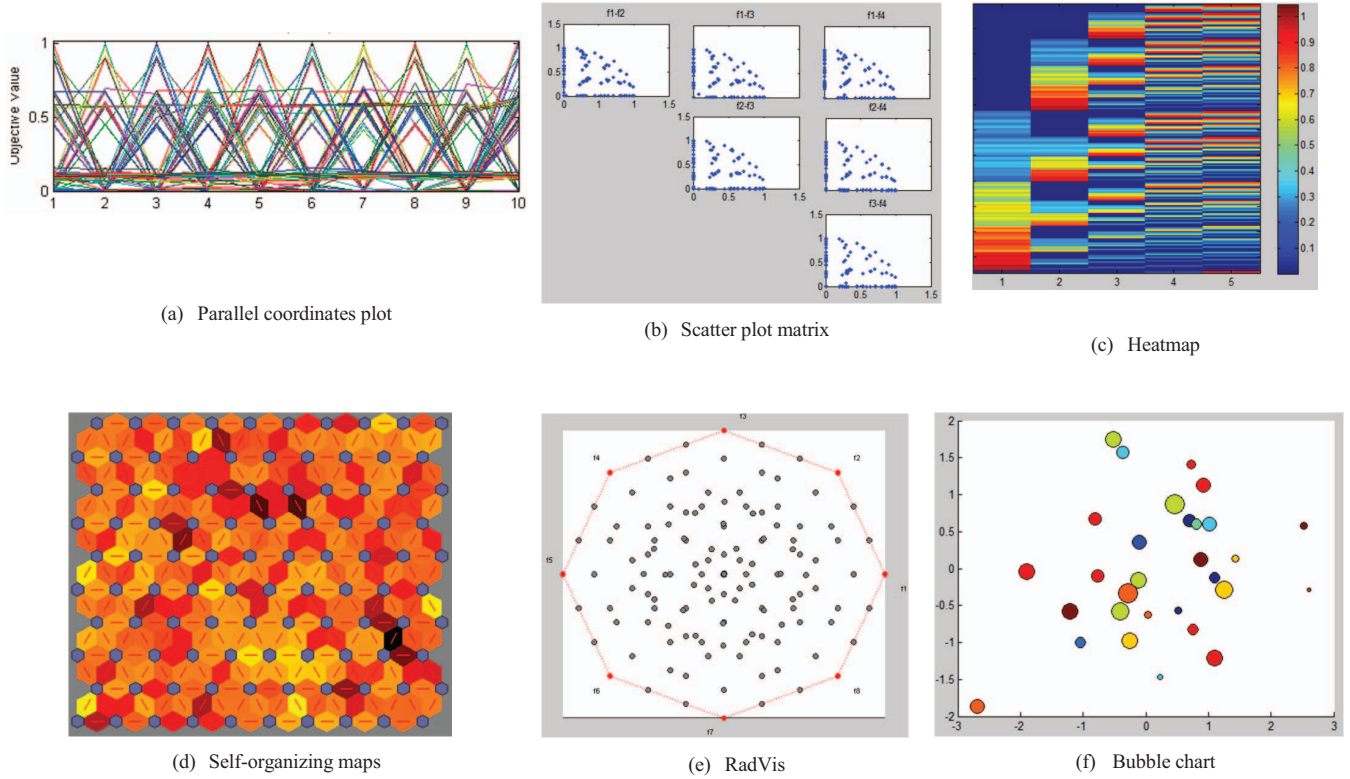(d) Self-organizing maps

(e) RadVis

(f) Bubble chart

Fig. 1. Visualization schemes used in many-objective optimization problems. (a) Parallel coordinates plot showing the performance of NSGA-III algorithm on 10-objective DTLZ4 test problem. (b) Scatter plot matrix showing linear and concave Pareto fronts for 4-objective problem. (c) Heatmap plot for 5-dimensional points. (d) Self-organizing map for 4-objective linear Pareto front. (e) RadVis/planer plot showing 10-objective DTLZ2 archived population. (f) Bubble chart representing four-dimensional values.

II. SURVEY OF VISUALIZATION METHODS USED IN MANY-OBJECTIVE OPTIMIZATION

In this section, we describe visualization techniques used in many-objective optimization.

A. Parallel Coordinate Plots

In many-objective optimization, parallel coordinates plot (PCP) [10] are a popular way to visualize the distribution, range, and trade-off among solutions of multi-dimensional objectives [25, 26]. An M-dimensional objective is represented by a polyline with vertices on M parallel axes placed along the x-axis. The parallel axes are M equidistant vertical bars along the x-axis for each objective. The y-axis corresponds to the range of values for each objective. Although parallel coordinate plots are not capable of showing the shape of the Pareto front, they are simple to construct, scale well to large numbers of objectives, and are a great visualization tool to show dependencies among objectives without the loss of data in the representation [27]. Fig. 1(a) shows a parallel coordinate plot for 10-objective DTLZ4 test problem.
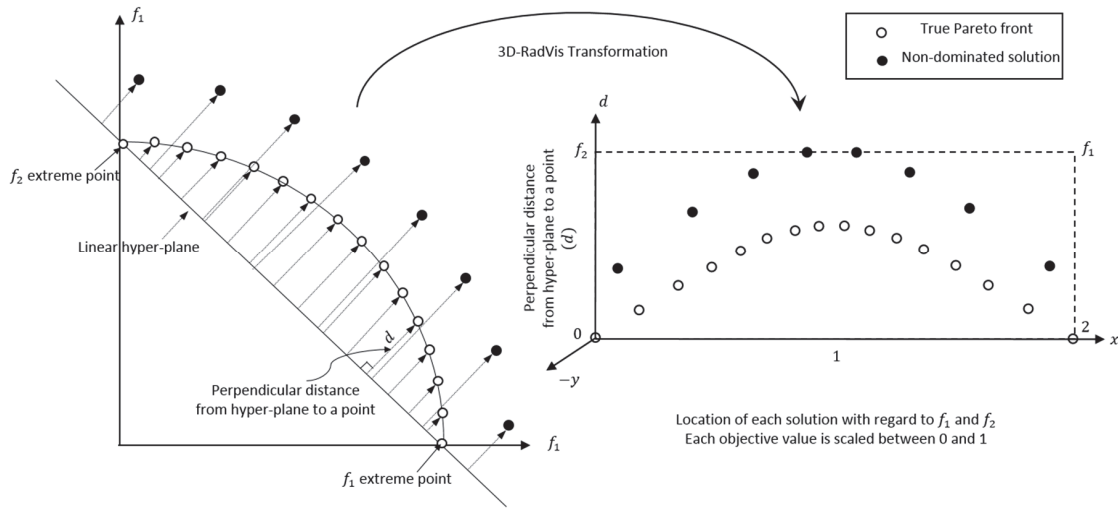
Fig. 2. Illustration of 3D-RadVis mapping process.

B. Scatter Plot Matrix

Given M-dimensional objective, scatter plot matrix plots all $\binom{M}{2}$ pairs of plots among M objectives [5, 28]. A scatter plot matrix is a simple visualization method capable of showing the pair-wise relationship of objectives while preserving some information on the shape of the Pareto front. When the number of objectives increases, the scatter plot matrix does not scale well as it requires a large space to show the relationship among pairs of each objectives. Fig. 1(b) shows approximate solutions obtained for 4-objective DTLZ4 problem.

C. Heatmap

Heatmap plots [11] are similar to the parallel coordinates plot, however objective values are shown using colors. Heatmap plots are very easy to construct and they can scale to visualize higher dimensional objectives. Moreover, similar to parallel coordinates plots it can show dependencies among objectives without the loss of data in the representation. However, Heatmap plots do not scale well when the number of solutions are large due to the number of colors used to represent each solution, and they cannot show the shape of the Pareto front. Fig. 1(c) shows a Heatmap plot showing approximate solutions obtained for 5-objective DTLZ2 problem.

D. Self-organizing Map (SOM)

Self-organizing maps (SOM) [13] are a type of artificial neural networks (ANN) trained using unsupervised learning to provide a mapping from M-dimensional objective to a low dimensional space (typically 2-D) [29]. SOMs consist of nodes (neurons) associated with a weight vector of the same dimension as the input data vectors or neurons. The nodes are arranged in a 2D space using a hexagonal or rectangular grid. SOMs commonly use the unified distance matrix (U-Matrix) [30] to store each node's average distance to its closest neighbors (different colors are used to represent each node's distance to adjacent nodes). Light areas represent clusters of similar neurons and dark areas indicate cluster boundaries. Fig.

1(d) shows approximate solutions obtained for 5-objective DTLZ4 problem.

E. Radial Coordinate Visualization (RadVis)

Radial coordinate visualization (RadVis) [14] maps M-dimensional points to a 2-dimensional space using a nonlinear mapping. Consider a point in 2-dimensional space connected to M equally spaced points on a circle with springs, where each dimension value is the spring constant for the corresponding spring. Now, if the 2-dimensional point is allowed to move and reach equilibrium, the location of this point will be the mapping of M-dimensional data points onto a 2-dimensional space. Fig. 1(e) shows RadVis/Planer plot showing approximate solutions obtained for 8-objective DTLZ4 problem. Although RadVis plots are not capable of showing the shape and convergence of the Pareto front, they are simple to construct, scale well to large numbers of objectives, and are a great visualization tool to show the distribution of solutions.

F. Bubble Chart

Bubble chart is similar to a 2- or 3-dimensional scatter chart, however data points are replaced with varying sizes of bubbles to represent the 3rd or 4th dimension. There is also a variation of bubble chart that use colored bubbles to represent the 4th or 5th dimension [31, 32]. Fig. 1(f) shows bubble chart to represent 3-dimensional values.

III. PROPOSED METHOD: 3D-RADVIS

The framework of the proposed 3D-RadVis visualization scheme is similar to RadVis; however, 3D-RadVis incorporates a third dimension to visualize the shape and convergence of an M-dimensional solution set. Consider an $N \times M$ non-dominated solution where N is the number of solutions and M is the dimension of the solution. 3D-RadVis involves two main steps: first, determining the distance of each solution from a reference hyper-plane, and second, mapping the location of M-dimensional solutions to a 2-dimensional xy plane.

Algorithm 1: 3D-RadVis (f) Procedure

Input: $f: N \times M$ non-dominated solutions, where M is the number of objectives and N is the number of solutions.

Output: $R: N \times 3$ transformation matrix for 3D-RadVis visualization

1: **for** $i = 1$ to M
2:     Sort using each objective value: $I = \texttt{sort}(f, i)$
3:     Compute extreme/boundary solution: $Z_i = I_1$
4: **end for**
5: Calculate the normal vector, a hyper-plane constructed by Z: $n = \texttt{norm}(Z)$
6: Calculate the constant, c for this plane: $c = (n \cdot Z_1)$
7: **for** $i = 1$ to N
8:     Calculate the perpendicular distance from n to solution i: $d = \frac{abs((f_i \cdot n) - c))}{\|n\|}$
9: **end for**
10: Normalize f by each objective: $f^{Norm} = \texttt{normalize}(f)$
11: Map f^{Norm} to 2D radial coordinates $[u_x, u_y] = \texttt{RadVis}(f^{Norm})$
12: $R = [u_x, u_y, d]$

To calculate the distance of each solution to the reference hyper-plane, we first sort these solutions using objective values and compute the extreme/boundary solution. For an M-dimensional solution set, we have M boundary solutions. Next, we construct a linear hyper-plane passing through these extreme points. The constructed hyper-plane is then used as the reference plane for each solution (point) in the solution set. Then, we compute the perpendicular distance (d) from the reference hyper-plane for each point, thereby preserving the shape and accuracy of the solution set. The values of d are used as the altitude (height or z-axis) of a solution in the 3D-RadVis mapping. Algorithm 1, lines 1 to 9 describe the above process.

Next, we utilize RadVis [14] scheme to determine the location of an M-dimensional solution onto a 2-dimensional xy plane (u_x, u_y). The first step is to normalize each solution per objective between 0 and 1. Now, consider an M-dimensional solution in a 2-dimensional space connected to M equally spaced points on a circle with springs, where each dimension value is the spring constant (K) for the corresponding spring. Now, if the 2-dimensional point is allowed to move and reach equilibrium, the location of this point will be the mapping of M-dimensional data point to the 2-dimensional space. Given $N \times M$ normalized non-dominated solutions (f^{Norm}), where M is the number of objectives and N is the number of solutions, solution i can be mapped to a 2D radial space as follows:

$$x_i = \frac{\sum_{j=1}^{M} f_{i,j}^{Norm} \cos(\theta_j)}{\sum_{j=1}^{M} f_{i,j}^{Norm}}, \tag{1}$$

and

$$y_i = \frac{\sum_{j=1}^{M} f_{i,j}^{Norm} \sin(\theta_j)}{\sum_{j=1}^{M} f_{i,j}^{Norm}} \tag{2}$$

where θ_j is the angular position on the circle corresponding to dimension j. The procedure is presented in Algorithm 2. Fig. 2 illustrates 3D-RadVis' mapping process.

Algorithm 2: RadVis (f^{Norm}) Procedure

Input: $f^{Norm}: N \times M$ normalized non-dominated solutions, where M is the number of objectives and N is the number of solutions.

Output: $[u_x, u_y]$ non-linear radial coordinates mapping of f^{Norm}

1: **for** $i = 1$ to N
2:     Calculate 2D radial location/mapping of normalized objective: $[x_i, y_i]$ Eqs.(1) and (2)
3: **end for**
4: $[u_x, u_y] = [x, y]$

IV. VISUALIZATION OF BENCHMARK TRUE AND APPROXIMATE PARETO FRONTS

In this section, we describe the test problems used, parameter settings of the NSGA-III algorithm [20], and visualization of these test problems using the proposed method, 3D-RadVis. To demonstrate the effectiveness of the proposed method, we used five many-objective benchmark problems containing a variety of Pareto front shapes (i.e., linear, concave, convex, mixed, and disconnected). In addition, we demonstrate the capability of 3D-RadVis to track the progress of the NSGA-III algorithm through generations visually.

A. Test Problems

In order to investigate the visualization capability of 3D-RadVis, we have used five many-objective benchmark test problems with various shapes. The benchmark problems are: DTLZ1, DTLZ2, convex DTLZ2, WFG1 and WFG2 [33, 34]. The number of variables are $(M + k - 1)$, where M is the number of objectives and $k = 5$ for DTLZ1, while $k = 10$ for DTLZ2 and convex DTLZ2. The corresponding Pareto-optimal fronts lie in $f_i \in [0, 0.5]$ for the DTLZ1 problem and in $f_i \in [0, 1]$ for DTLZ2 and convex DTLZ2 problems. For WFG1 and WFG2 test problems, the number of position parameters is set to $k = M$, where M is the number of objectives and the number of distance parameters is set to $l = 3$ for all dimensions. The Pareto-optimal fronts for WFG test problems used in this work lie in $f_i \in [0, 2i]$. Table I presents detailed characteristics of the test problems utilized in this study.

TABLE I.   TEST PROBLEMS

Problem	Characteristics
DTLZ1	Linear, Multimodal
DTLZ2	Concave
Convex DTLZ2	Convex
WFG1	Convex, Mixed, Biased
WFG2	Convex, Disconnected, Multimodal

B. Parameters Setting

In order to investigate the visualization capability of 3D-RadVis when two or more Pareto fronts are involved (e.g., true Pareto front and approximate Pareto front), we have used non-dominated solutions obtained by the NSGA-III algorithm for 5-

and 8-objective DTLZ1, DTLZ2 and convex DTLZ2 problems. Table II presents parameter settings used by NSGA-III and Table III shows the number of reference points (H), the population size (N), and the number of inner and outer divisions used for different dimensions of the test problems. Table IV shows the maximum generation used for solving these test problems.

Parameters	NSGA-III
SBX probability (p_c)	0.9
Polynomial mutation (p_m)	$1/n$
Crossover Distribution Index (η_c)	30
Mutation Distribution Index (η_m)	20

C. 3D-RadVis Visualization of Test Problems

Here, we investigate how well 3D-RadVis maps 2-, 3-, 4-, 5-, and 8-objective Pareto fronts to a 3-D space. Note that since we can map 2-D data points on to x-axis the u_y value always set to zero. Fig. 3(a) depicts the mapping of 2-D DTLZ1 onto a 3-D space. Since all the points lie on the reference hyper-plane, the value of d is zero. Fig. 3(b) shows the mapping of 2-objective DTLZ2 onto a 3-D space. Here we see that the shape of DTLZ2 is similar to a quarter circle centered at (0, 0), the largest distant point from the reference hyper-plane is located at the center of the arc. Fig. 3(c) shows the mapping of 2-objective convex DTLZ2 onto a 3-D space. Here we can see that the lowest point on the 3D-RadVis plot is located close to f_1, and this is because the Pareto-optimal surface of the convex DTLZ2 problem has sharp decent close to the intermediate f_1 region. Fig. 3(d) shows the mapping of 2-objective WFG1 test problem onto a 3-D space RadVis. It can be seen that 3D-RadVis is able to map the mixed Pareto-optimal surface to a 3-D space. Fig. 3(e) shows the mapping of the WFG2 test problem. Similar to the previous test problems, 3D-RadVis is able to capture the shape of relative locations of disconnected Pareto-optimal fronts of the WFG2 problem. In all test problems, 3D-RadVis is able to capture all features of the test problems regardless of shape or sharp/slow changes in the Pareto-optimal front.
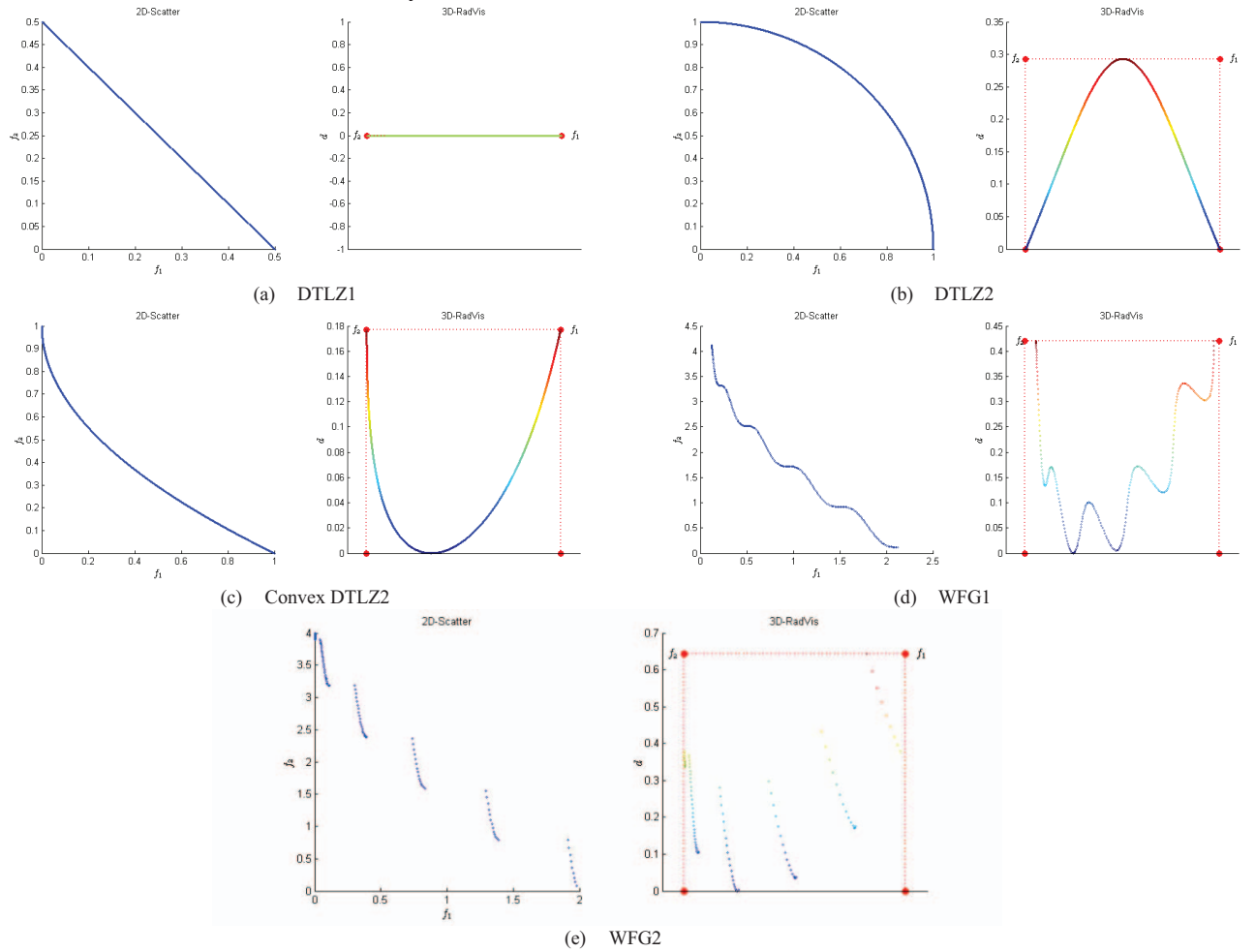

(a) DTLZ1   (b) DTLZ2   (c) Convex DTLZ2   (d) WFG1   (e) WFG2

Fig. 3.   3D-RadVis plots of 2-objective linear (DTLZ1), concave (DTLZ2), convex (convex DTLZ2), mixed (WFG1) disconnnected (WFG2) Pareto fronts.

(a) DTLZ1   (b) DTLZ2
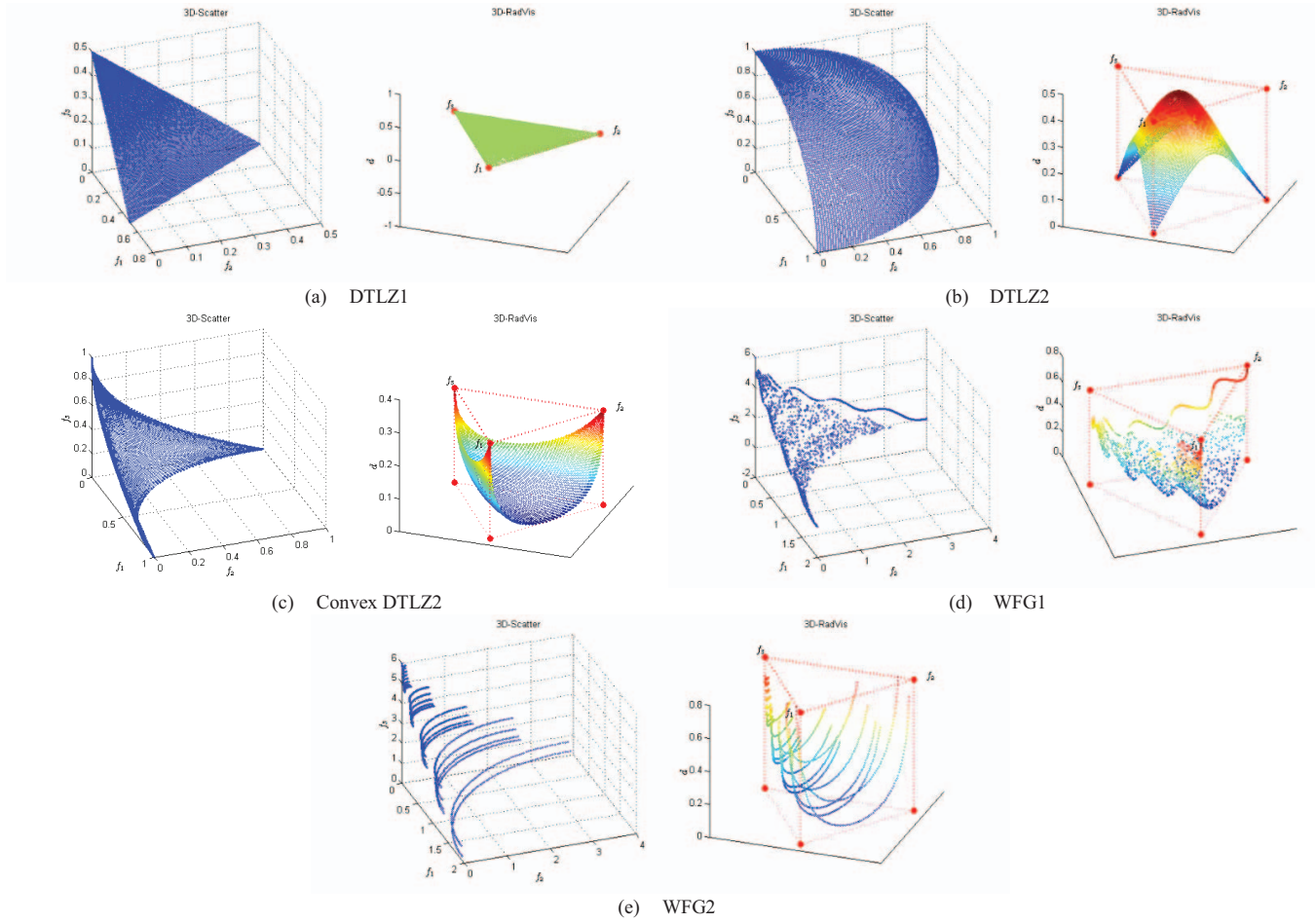
(c) Convex DTLZ2   (d) WFG1

(e) WFG2

Fig. 4. 3D-RadVis plots of 3-objective linear (DTLZ1), concave (DTLZ2), convex (convex DTLZ2), mixed (WFG1) disconnected (WFG2) Pareto fronts.

TABLE III. NUMBER OF REFERENCE POINTS AND POPULATION SIZES USED IN NSGA-III.

Number of Objectives (M)	Divisions		Reference Points(H)	Population Size (N)
	Outer	Inner		
5	6	0	210	212
8	3	2	156	156

TABLE IV. MAXIMUM NUMBER OF GENERATIONS USED IN DIFFERENT TEST PROBLEMS.

Problem	M	Max Gen
DTLZ1	5	750
	8	2000
DTLZ2	5	750
	8	2000
Convex DTLZ2	5	750
	8	2000

Fig. 4 demonstrates the effectiveness of 3D-RadVis in mapping 3-objective test problems to 3-D space while preserving all characteristics of the test problems. Fig. 5 shows the mapping of 4-, 5- and 8-objective DTLZ2 and convex DTLZ2 test problem onto 3-D spaces. As it can be seen from

these diagrams, 3D-RadVis is able to precisely map and visualize all aspects of higher dimensional problems.

D. 3D-RadVis Visualization of Approximate Pareto Fronts

The previous section has shown the effectiveness of 3D-RadVis to visualize the true Pareto-optimal fronts when the number of objectives are three or more. In this section, we show how researchers can utilize 3D-RadVis to investigate the performance of an algorithm. In the current experiment, we have used the NSGA-III algorithm to solve 5- and 8-objective DTLZ1, DTLZ2, and convex DTLZ3 test problems. Tables II to IV show parameter settings, population size, number of reference points and maximum number of generations used in these experiments.

Fig. 6 shows the performance of NSGA-III for 5- and 8-objective DTLZ1 test problem. From the 3D-RadVis plot, we can precisely see how close the obtained solutions are to the true Pareto front. For example, Fig. 6(b) shows that the worst (based on distance) solution is $d = 10^{-3}$ far from the true front. The top view of 3D-RadVis plot shows that NSGA-III is able to uniformly distribute the solution on the entire front. Fig. 7 shows the performance of NSGA-III for 5- and 8-objective DTLZ2 test problem. While the convergence and distribution
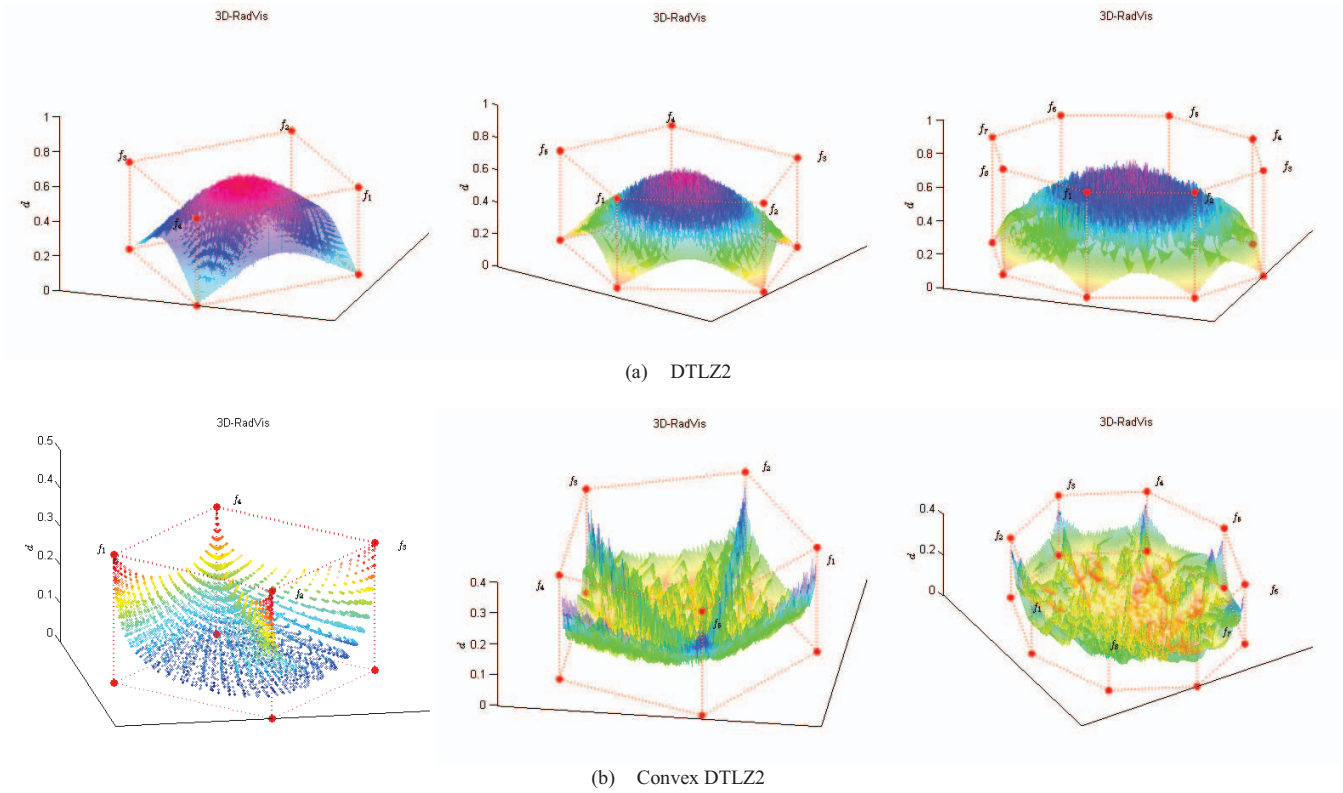
(a) DTLZ2

(b) Convex DTLZ2

Fig. 5.   3D-RadVis plots of 4-, 5- and 8-objective linear (DTLZ1), concave (DTLZ2), and convex (convex DTLZ2) Pareto fronts.

(a)   5- objective DTLZ1
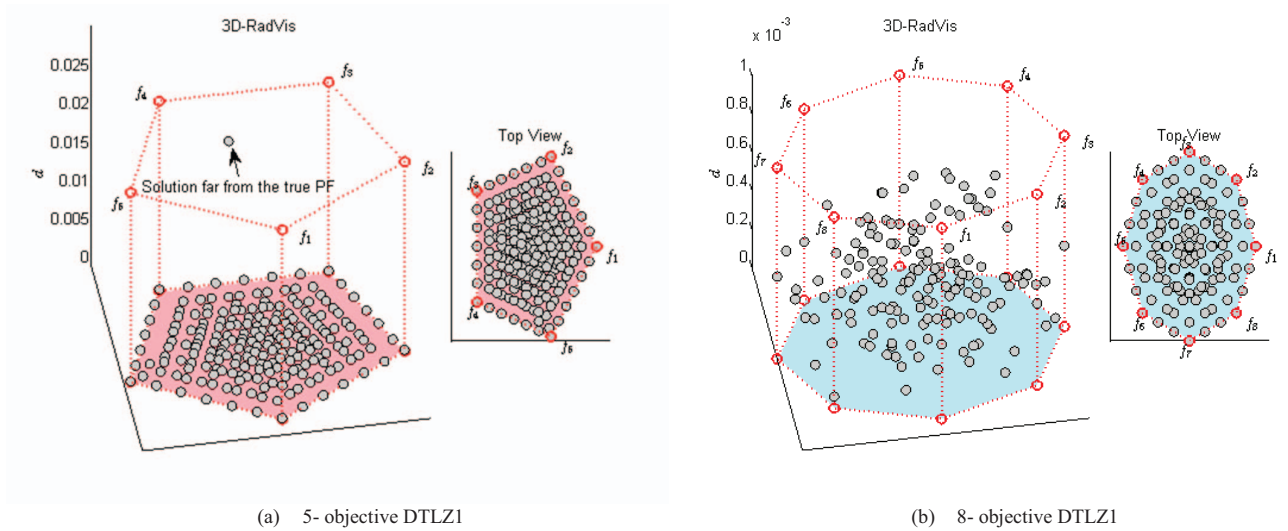
(b)   8- objective DTLZ1

Fig. 6.   3D-RadVis plots showing obtained solutions by NSGA-III for 5- and 8-objective DTLZ1 test problem.

of the obtained solutions are close to the true Pareto front, when examining the performance of NSGA-III on 8-objective convex DTLZ2 problem, NSGA-III is not able to find well distributed solutions on the entire Pareto front (see Fig. 8).

3D-RadVis can also effectively be used by researchers and decision makers to explore and understand the search behavior of an algorithm at each generation. They can take advantage of the visualization power of 3D-RadVis to gain useful information regarding an algorithm and improve their search

2016 IEEE Congress on Evolutionary Computation (CEC)

ability and ultimately develop new optimization algorithms. Furthermore, in an interactive environment it is possible to rotate and visualize solutions from different viewpoints to better understand the relationships among solutions. Fig. 9 shows the performance of NSGA-III for 5-objective DTLZ2

test problem after 25, 50, 100 and 250 generations. For the 3D-RadVis plots, we can see that NSGA-III is able to converge while maintaining well a distributed solution through generations
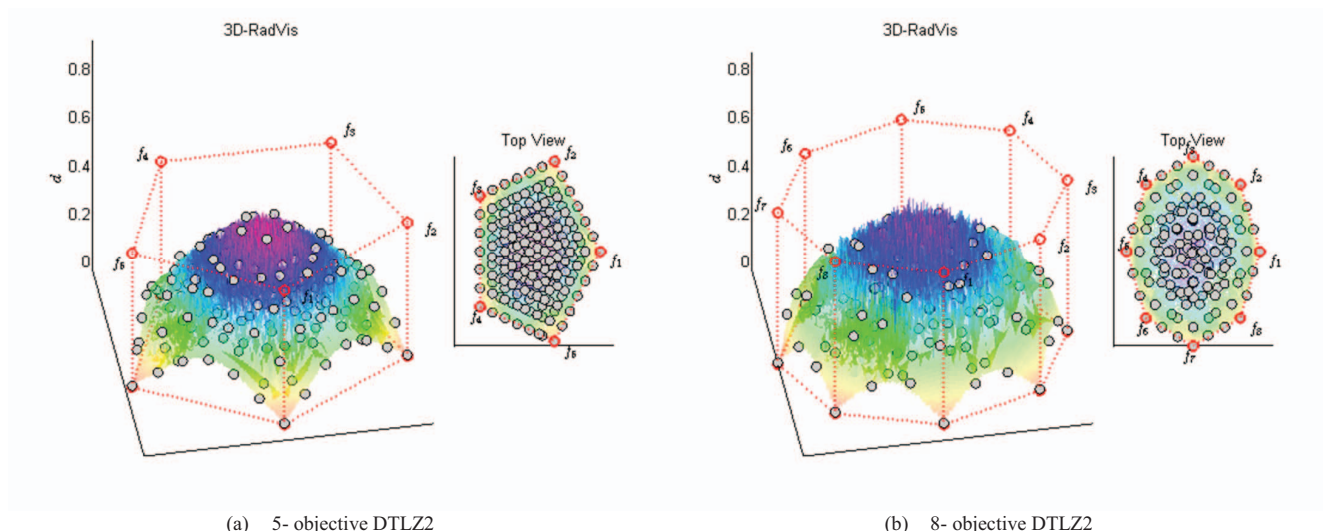

| (a)   5- objective DTLZ2 | (b)   8- objective DTLZ2 |

Fig. 7.   3D-RadVis plots showing obtained solutions by NSGA-III for 5- and 8-objective DTLZ2 test problem.

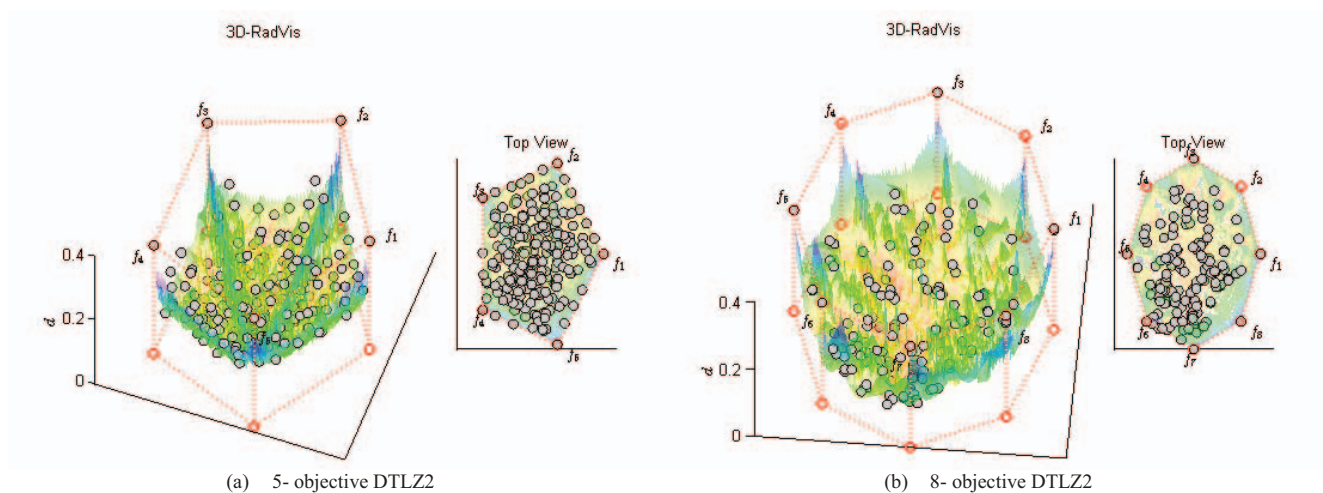| (a)   5- objective DTLZ2 | (b)   8- objective DTLZ2 |

Fig. 8.   3D-RadVis plots showing obtained solutions by NSGA-III for 5- and 8-objective convex DTLZ2 test problem.

(a)   25 generations

(b)   50 generations

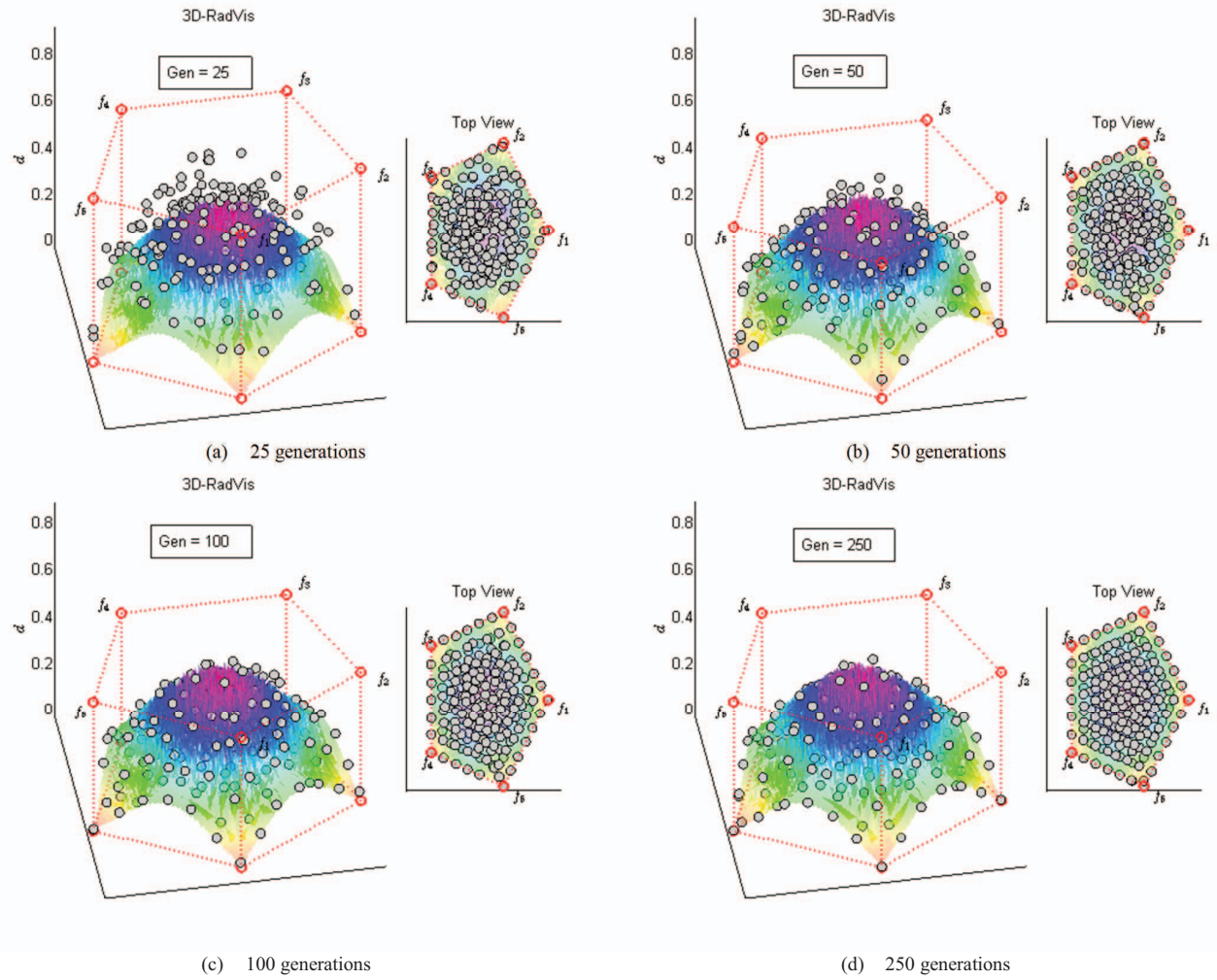(c)   100 generations

(d)   250 generations

Fig. 9. 3D-RadVis plots showing the progress of obatined solutions by NSGA-III for 5-objective DTLZ2 test problem after 25, 50, 100, and 250 generations.

V. CONCLUSION REMARKS

In this paper, we proposed a fast and powerful 3-D visualization method called, 3D-RadVis. This method uses a radial coordinate system to map $M-$dimensional objectives space to a 2-D space (u_x, u_y) and a distance metric (d) to maintain the location of each non-dominated solution from a reference hyper-plane constructed using the extreme points of the Pareto-optimal front. The radial coordinates, (u_x, u_y), show the distribution of the solution and the combination of these radial coordinates with the distance metric d, show the shape and accuracy of the solution.

From the experimental tests on widely used many-objective optimization test problems, 3D-RadVis is able to precisely show the shape, distribution, and convergence of complex Pareto fronts (linear, concave, convex, mixed, and disconnected). Moreover, 3D-RadVis can be scaled to higher dimensions and is capable of showing multiple Pareto fronts simultaneously (e.g. true Pareto front and approximate solutions). It can effectively be used by researchers and decision makers to explore and understand the search behavior of an algorithm at each generation whereby gaining useful information regarding an algorithm to improve their search ability and ultimately development of new optimization algorithms. 3D-RadVis can also be utilized by decision-makers to observe the relative location of a solution, evaluate trade-off among objectives, and select preferred solutions. For an improved navigation, decision-makers can use immersive virtual technologies, such as the CAVE, to easily visualize the entire Pareto front from the 3D-RadVis plot and select the ideal solution according to their requirement and budget.

Since 3D-RadVis maps M-dimensional objective to a 3-D map while preserving the shape, distribution and accuracy of the solution, it is natural to develop a new performance metric capable of measuring the convergence and diversity of approximated Pareto-optimal solutions. Therefore, in the future, we would like to extend this study to investigate how 3D-RadVis-based performance metric can be consistent with other performance metrics which are currently used in many-objective optimization.

REFERENCES

[1] E. J. Hughes, "Evolutionary many-objective optimisation: many once or one many?," in Evolutionary Computation, 2005. The 2005 IEEE Congress on, pp. 222-227, 2005.

[2] J. Knowles and D. Corne, "Quantifying the effects of objective space dimension in evolutionary multiobjective optimization," in Evolutionary Multi-Criterion Optimization, pp. 757-771, 2007.

[3] Z. He and G. Yen, "Many-Objective Evolutionary Algorithm: Objective Space Reduction+ Diversity Improvement," 2012.

[4] Z. He, G. G. Yen, and J. Zhang, "Fuzzy-based Pareto optimality for many-objective evolutionary algorithms," Evolutionary Computation, IEEE Transactions on, vol. 18, pp. 269-285, 2014.

[5] K. Deb, Multi-objective optimization using evolutionary algorithms vol. 16: John Wiley & Sons, 2001.

[6] M. Garza-Fabre, G. T. Pulido, and C. A. C. Coello, "Ranking methods for many-objective optimization," in MICAI 2009: Advances in Artificial Intelligence, ed: Springer, pp. 633-645, 2009.

[7] H. Ishibuchi, Y. Tanigaki, H. Masuda, and Y. Nojima, "Distance-Based Analysis of Crossover Operators for Many-Objective Knapsack Problems," in Parallel Problem Solving from Nature–PPSN XIII, ed: Springer, pp. 600-610, 2014.

[8] H. Sato, H. Aguirre, and K. Tanaka, "Variable space diversity, crossover and mutation in MOEA solving many-objective knapsack problems," Annals of Mathematics and Artificial Intelligence, vol. 68, pp. 197-224, 2013.

[9] A. López Jaimes and C. A. Coello Coello, "Some techniques to deal with many-objective problems," in Proceedings of the 11th Annual Conference Companion on Genetic and Evolutionary Computation Conference: Late Breaking Papers, pp. 2693-2696, 2009.

[10] A. Inselberg, "The plane with parallel coordinates," The Visual Computer, vol. 1, pp. 69-91, 1985.

[11] A. Pryke, S. Mostaghim, and A. Nazemi, "Heatmap visualization of population based multi objective algorithms," in Evolutionary multi-criterion optimization, pp. 361-375, 2007.

[12] D. J. Walker, R. M. Everson, and J. E. Fieldsend, "Visualizing mutually nondominating solution sets in many-objective optimization," Evolutionary Computation, IEEE Transactions on, vol. 17, pp. 165-184, 2013.

[13] T. Kohonen, "Self-organizing maps, vol. 30 of Springer Series in Information Sciences," ed: Springer Berlin, 2001.

[14] P. Hoffman, G. Grinstein, K. Marx, I. Grosse, and E. Stanley, "DNA visual and analytic data mining," in Visualization'97., Proceedings, pp. 437-441, 1997.

[15] S. D. Miyahira, R. A. Folen, M. Stetz, A. Rizzo, and M. M. Kawasaki, "Use of immersive virtual reality for treating anger," Stud Health Technol Inform, vol. 154, pp. 82-86, 2010.

[16] C. A. Kilmon, L. Brown, S. Ghosh, and A. Mikitiuk, "Immersive virtual reality simulations in nursing education," Nursing education perspectives, vol. 31, pp. 314-317, 2010.

[17] M. Carrozzino and M. Bergamasco, "Beyond virtual museums: Experiencing immersive virtual reality in real museums," Journal of Cultural Heritage, vol. 11, pp. 452-458, 2010.

[18] B. Bideau, R. Kulpa, N. Vignais, S. Brault, F. Multon, and C. Craig, "Using virtual reality to analyze sports performance," Computer graphics and applications, IEEE, vol. 30, pp. 14-21, 2010.

[19] S. Manjrekar, S. Sandilya, D. Bhosale, S. Kanchi, A. Pitkar, and M. Gondhalekar, "CAVE: An Emerging Immersive Technology--A Review," in Computer Modelling and Simulation (UKSim), 2014 UKSim-AMSS 16th International Conference on, pp. 131-136, 2014.

[20] K. Deb and H. Jain, "An evolutionary many-objective optimization algorithm using reference-point-based nondominated sorting approach, part I: solving problems with box constraints," Evolutionary Computation, IEEE Transactions on, vol. 18, pp. 577-601, 2014.

[21] T. Tusar and B. Filipic, "Visualization of Pareto front approximations in evolutionary multiobjective optimization: A critical review and the prosection method," Evolutionary Computation, IEEE Transactions on, vol. 19, pp. 225-245, 2015.

[22] Z. He and G. Yen, "Visualization and performance metric in many-objective optimization," 2015.

[23] D. Walker, J. Fieldsend, and R. Everson, "Visualising many-objective populations," in Proceedings of the 14th annual conference companion on Genetic and evolutionary computation, pp. 451-458, 2012.

[24] H. Borhan and E. Hodzen, "A Robust Design Optimization Framework for Systematic Model-Based Calibration of Engine Control Systems," Journal of Engineering for Gas Turbines and Power, vol. 137, p. 111601, 2015.

[25] A. Inselberg, Parallel coordinates: Springer, 2009.

[26] C. M. Fonseca and P. J. Fleming, "Multiobjective optimization and multiple constraint handling with evolutionary algorithms. II. Application example," Systems, Man and Cybernetics, Part A: Systems and Humans, IEEE Transactions on, vol. 28, pp. 38-47, 1998.

[27] P. J. Fleming, R. C. Purshouse, and R. J. Lygoe, "Many-objective optimization: An engineering design perspective," in Evolutionary multi-criterion optimization, pp. 14-32, 2005.

[28] D. Carr and W. Nicholson, "Evaluation of graphical techniques for data in dimensions 3 to 5: scatter plot matrix, glyph and stereo examples," Pacific Northwest Labs., Richland, WA (USA), 1985.

[29] S. Obayashi and D. Sasaki, "Visualization and data mining of Pareto solutions using self-organizing map," in Evolutionary multi-criterion optimization, pp. 796-809, 2003.

[30] A. Ultsch, U*-matrix: a tool to visualize clusters in high dimensional data: Fachbereich Mathematik und Informatik Berlin, 2003.

[31] M. Ashby, "Multi-objective optimization in material design and selection," Acta materialia, vol. 48, pp. 359-369, 2000.

[32] S. Poles, P. Geremia, F. Campos, S. Weston, and M. Islam, "MOGA-II for an automotive cooling duct optimization on distributed resources," in Evolutionary Multi-Criterion Optimization, pp. 633-644, 2007.

[33] K. Deb, L. Thiele, M. Laumanns, and E. Zitzler, "Scalable multi-objective optimization test problems," in Proceedings of the Congress on Evolutionary Computation (CEC-2002),(Honolulu, USA), pp. 825-830, 2002.

[34] S. Huband, L. Barone, L. While, and P. Hingston, "A scalable multi-objective test problem toolkit," in Evolutionary multi-criterion optimization, pp. 280-295, 2005.